Itavastatin and Resveratrol increase triosephosphate isomerase protein (TPI) in a newly identified variant, TPIQ181P, that confers TPI deficiency

Andrew P. VanDemark[A, ≠], Stacy L. Hrizo[B,C,D], Samantha L. Eicher[B,C], Jules Kowalski[A], Tracey D. Myers[B,C], Megan R. Pfeifer [B,C], Kacie N. Riley[E], Dwight D. Koeberl[E], and Michael J. Palladino[A,B,≠]

[A] Biological Sciences and Structural Biology, University of Pittsburgh, Pittsburgh, PA 15260, USA

[B] Department of Pharmacology & Chemical Biology, University of Pittsburgh School of Medicine, Pittsburgh, PA 15261

[C] Pittsburgh Institute for Neurodegenerative Diseases, University of Pittsburgh School of Medicine Pittsburgh, PA 15261

[D] Department of Biology, Slippery Rock University of Pennsylvania, Slippery Rock, PA 16057

[E] Department of Pediatrics, Division of Medical Genetics, Duke University Medical Center Durham, NC 27710

[≠] Corresponding authors: Michael J. Palladino (mjp44@pitt.edu) & Andrew VanDemark (andyv@pitt.edu)

Abstract:

TPI Deficiency (TPI Df) is an untreatable glycolytic enzymopathy that results in hemolytic anemia, progressive muscular impairment and irreversible brain damage. Although there is a "common" mutation (*TPI*^{E105D}), other pathogenic mutations have been described. We identified patients with who are compound heterozygous for a newly-described mutation, *TPI*^{Q181P}, and the common *TPI*^{E105D} mutation. Intriguingly, these patients lack neuropathy or cognitive impairment. We initiated biochemical and structural studies of TPI^{Q181P}. Surprisingly, purified TPI^{Q181P} protein has markedly impaired catalytic properties while crystallographic studies demonstrate that TPI^{Q181P} results in a highly disordered catalytic lid. We propose that genetic complementation is occurring between the two alleles, one with little activity (*TPI*^{Q181P}) and one

Disease Models & Mechanisms • DMM • Accepted manuscript

with low stability (*TPI*^{E105D}). Consistent with this, *TPI*$^{Q181P/E105D}$ fibroblasts exhibit a significant reduction in TPI protein but much higher protein than *TPI*$^{E105D/E105D}$ fibroblasts. These data suggest that impaired stability, and not catalytic activity, is a better predictor of TPI Df severity. Lastly, we tested two recently discovered chemical modulators of mutant TPI stability and observed a significant increase in TPI in *TPI*$^{Q181P/E105D}$ patient cells.

Introduction

Triosephosphate Isomerase deficiency (TPI Df) is a severe genetic metabolic disorder which presents early on in childhood. Typically, TPI Df patients are born healthy but hemolytic anemia leads to recurrent infections. The patient experiences developmental delays and a rapidly progressive disease course with symptoms related to muscle weakness and neurological impairment. Muscle weakness and wasting impairs locomotor function (limb and core muscles) as well as breathing in some cases (diaphragm). The disease typically further progresses resulting in severe and irreversible neurologic pathology and early death. Currently, there are no drug treatments for TPI Df. Patients are provided support for their symptoms and often diet and nutrient support that is of unknown clinical value. Thus, the prognosis remains grim, and few patients survive to adulthood.

TPI Df can be caused by a handful of pathogenic missense mutations that result in specific amino acid substitutions in TPI, the most common of which is *TPI*^{E105D}. Numerous TPI Df-causing pathogenic mutations have been studied and, thus far, pathogenic mutations encode proteins that retain function (at least some) but typically are unstable leading to protein degradation and lowered TPI levels. We have identified a novel TPI Df variant, *TPI*^{Q181P}, that has an atypical and less severe disease course. The mutation was found in two compound heterozygous sibling patients with the common mutation. The *TPI*$^{Q181P/E105D}$ patients we observed have severe skeletal muscle symptoms, however, their anemia is relatively mild and their cognitive function has remained normal even into adulthood.

TPI is a homodimer with each monomer adopting the $(\beta\alpha)_8$ TIM barrel fold (Banner, Bloomer, Petsko, Phillips, & Pogson, 1972; Lolis et al., 1990). Access to the catalytic site is restricted by the catalytic lid which is formed by loop 6. The catalytic lid is dynamic and has been observed in both open and closed states (Wierenga, Noble, & Davenport, 1992). Transitions between the open and closed state of the catalytic lid are coordinated with changes in the positions of prominent residues within the active site including E165, K13, H95, and S96 (Massi, Wang, & Palmer, 2006; Wierenga et al., 1992; Zhang et al., 1994). Numerous structures

have been solved for wild type and mutant TPI, including several mutant disease-associated proteins (Roland et al., 2015; Roland et al., 2019). TPI^{E105D} exhibits altered solvation and reduced stability of the TPI dimer (Rodriguez-Almazan et al., 2008), while the catalytic lid and active site residues within the TPI^{I170V} mutant resemble the closed state (Roland et al., 2015). Recently, we have reported the structure of TPI^{R190Q} which is positioned distant from the active site, where it coordinates two salt bridge interactions that are critical for protein stability. The loss of these interactions also confered an altered arrangement of catalytic site residues. Overall, these studies have highlighted the tight coordination between the active site and the conformation and dynamics of the catalytic lid.

To date, animal studies of TPI in the mouse have not effectively modeled TPI Df (Conway et al., 2018; Pretsch, 2009; Segal et al., 2019), and most studies of pathogenesis have been conducted in the fruit fly *Drosophila* (Celotto, Frank, Seigle, & Palladino, 2006; Hrizo et al., 2013; Hrizo & Palladino, 2010; Roland et al., 2013; Roland et al., 2016; Seigle, Celotto, & Palladino, 2008). One particularly informative mouse study concluded that a mutation that does not grossly impair stability, even though it significantly impairs catalytic function, fails to result in neuromuscular impairment and thus does not model TPI Df well (Segal et al., 2019). *Drosophila* with a unique mutation known as *TPI$^{sugarkill\ (sgk)}$* appear to model neuromuscular aspects of the disease well and were the first model organism of this disease (Celotto et al., 2006). One study with *TPI^{sugarkill}* generated compound heterozygotes with a catalytically inactive allele, *TPI$^{sgk/deltaCat}$*, and the animals were suprisingly less-severely affected than homozygous *TPI^{sgk}* animals (Roland et al., 2013). The animals were not unaffected and still had neuromuscular impariment but locomotor function was significantly improved and the compound heterozygous animals did live significantly longer (Roland et al., 2013). This was the first report of genetic complementation between two *TPI* alleles, albeit incomplete complementation. The conclusion was that TPI^{sgk} retained significant amounts of activity but the protein itself was unstable and rapidly degraded, whereas, TPI^{deltaCat} was known to ablate activity but was relatively stable. Thus, the combination was less affected due to partial genetic complementation between these alleles.

Although there is some variability in the TPI Df disease course that is not completely understood, there is a preponderance of evidence with numerous pathogenic mutations that supports the conclusions that 1) pathogenic variants retain significant activity, 2) TPI Df mutant proteins exhibit reduced stability presumably due to accelerated turnover by protein quality control (PQC) machinery, and 3) impaired stability and not activity correlates best with disease

severity. As such, we and others have proposed that impairing mutant TPI turnover is the most promising avenue for the development TPI Df treatments (Hrizo et al., 2021; Segal et al., 2019; Vogt et al., 2021). Recent studies have utilized RNAi genetic screens to identify potential therapeutic targets (Hrizo et al., 2021) and exploited human cellular models and developed high-throughput optical screens to enable direct drug screening for novel TPI Df therapeutics (Vogt et al., 2021). Interestingly, these studies have identified two compounds, resveratrol and itavastatin, that increase the common mutant TPI protein levels a human cellular TPI Df model and also in TPI Df patient cells (Vogt et al., 2021). Here we report that these compounds also increase protein levels in *TPI*$^{Q181P/E105D}$ patient fibroblasts, suggesting these compounds should be tested for efficacy in animal models as they would represent a first-ever treatment for TPI Df. Importantly, the *in vitro* patient cellular data suggest that these compounds could benefit not only patients with the common mutation but compound heterozygous patients such as are reported here.

Results

Clinical Descriptions

Two siblings with childhood-onset locomotor impariment were identified and evaluated clinically for metabolic disease and possible TPI Df.

Patient 1: A 21y.o. female with a history of developmental delay, spastic diplegia, and cerebellar ataxia was seen. The patient was the product of a full-term, normal vaginal delivery with no complications. She was developing normally until the age of 10 months, when development seemed to regress after a fall resulting in injury to her head. The parents reported she was back on track by 12 months and walked at approximately 18 months, but with a noticeably abnormal gait and upper body posture. Dystonia and tightness of her left side, as well as tremor in her hands was appreciated around the same time. Gross motor delays persisted, and patient continues to have spasticity and dystonic posturing in the lower extremities, as well as slurring of her speech.

As part of her work-up, she had a thorough evaluation that included muscle biopsy and oxidative phosphorylation studies in 2007, which identified a mitochondrial complex I deficiency, though no molecular genetic etiology was identified. She had been placed on coenzyme Q10 and reports today that she could not tell any change when she was taking it.

On review of systems, the patient denies anemia, pallor, jaundice (other than during the newborn age), muscle atrophy, or seizures. She does acknowledge fatigue, spasms, intention tremor, and dystonia. The patient receives Botox for tightness in her neck and left arm and also feels tightness in her shoulders. She reports being on continuous positive airway pressure (CPAP) at night for both muscle weakness and central apnea. Cognitive function is normal although speech is hard to understand due to hyper-nasality. The patient communicates well using assistive devices and appears to be at age level for reading and comprehension.

Patient 2: The patient is a 17y.o. male with a history of dystonia, cerebellar ataxia, speech delay, unsteadiness and tremor, and hypotonia and is patient 1's sibling. He presented in early childhood with ataxia, tremors, and dystonia. Patient 2's early development was mostly on track, though parents report that he sat a little late, but are not sure the exact age. He was walking between 13-14 months, but reportedly had an abnormal gait, similar to his sister, and seemed to use posturing to maintain balance. Patient 2 spoke his first words around 18 months of age and received speech therapy. He made fast progress in speech per report.

Like his sister, patient 2 carried a diagnosis of mitochondrial complex I deficiency based on reduced activity identified on electron transport chain testing completed in 2007, but no nuclear or mitochondrial gene mutations were identified as etiology for the complex I deficiency.

On review of systems, patient 2 and his parents deny anemia, pallor, dystonia, seizures and cardiomyopathy. They acknowledge some fatigue, intention tremor, and spasms. They note that he has muscle atrophy and explain that because his feet were "turning in" he had surgical correction that made it difficult to stand or walk (his family attributes his muscle atrophy in calves and thighs to difficulty standing/walking after this procedure). His past medical history is also notable for surgery at 15yo due to his lower jaw protruding. His family explains that he uses Trilogy at night due to muscle weakness and central apnea. As with patient 1, cognitive function appears normal, but speech suffers from hyper-nasality and the patient communicates well will assistive devices. The patient appears to be at age level for reading and comprehension.

Mutational Analyses

Both patients were found to be compound heterozygous for two *TPI* variants (*c.315G>C; p.E105D and c.542A>C; p.Q181P*) via whole exome sequencing done at GeneDx in 2014. The TPI^{E105D} variant is seen in about 80% of variant alleles in patients with clinical TPI deficiency,

and *TPI*^{Q181P} is classified as a variant of uncertain significance. Patient fibroblasts were obtained from both patients and both parents and the *TPI* locus was PCR amplified and coding regions were sequenced. These studies confirmed that *TPI*^{Q181P} and *TPI*^{E105D} are the only mutations present, both patients are compound heterozygotes for these alleles, and that the *TPI*^{E105D} variant was paternally inherited (parent 2) while the *TPI*^{Q181P} was inherited maternally (parent 1; Figure 1). While the adenine to cytosine transversion is a missense mutation resulting in a Q181P amino acid substitution, it also affects the -2 position relative to the exon 5 splice donor in pre-mRNA. RT-PCR was performed and exon skipping was not evident, consistent with the expression of TPI^{Q181P} protein (Supplemental Figure 1).

Q181P protein biochemistry

To better understand the significance of the *TPI*^{Q181P} mutation, recombinant human TPI^{Q181P} and TPI^{WT} proteins were purified for biochemical studies as in (Roland et al., 2019). TPI activity was measured using a well-established NADH-linked assay (Roland et al., 2013; Williams et al., 1999). When enzyme activity of TPI^{Q181P} was directly compared to the wildtype TPI, a significant reduction in both V_{max} and K_{cat} were observed (Figure 2). These studies demonstrate the TPI^{Q181P} enzyme has less than 9% of the catalytic turnover rate (Kcat/Km) of the wildtype TPI enzyme. These are significant changes in enzyme function in comparison to the E105D "common" mutation in which the E105D homodimer exhibited 75-97% activity by Kcat/Km measurements compared to the wildtype enzyme in three different published studies (Cabrera, Torres-Larios, Garcia-Torres, Enriquez-Flores, & Perez-Montfort, 2018; De La Mora-De La Mora et al., 2013; Rodriguez-Almazan et al., 2008). The changes observed in the Q181P TPI enzyme activity are more similar to the activity observed for G72A and V231M which exhibited ~23% and ~11.2% activity by kcat/km respectively (Cabrera et al., 2018). The K_m of the TPI^{Q181P} mutant enzyme also significantly increased ~ 3-fold over wildtype TPI indicating that TPI^{Q181P} exhibits reduced substrate binding affinity compared to the wildtype enzyme. The more common E105D TPI mutant exhibited no significant reported change in Km in two separate studies and a less than two-fold increase in a third study (Cabrera et al., 2018; De La Mora-De La Mora et al., 2013; Rodriguez-Almazan et al., 2008). However, again the G72A and V213M mutations exhibited an increase Km of ~6.5-fold and ~8.7-fold respectively. This suggests the G72A and V231M mutations are more similar to Q181P than the E105D allele in that they both exhibit significant reductions in catalytic activity coupled with reduced substrate affinity (Cabrera et al.,

2018). We also examined the thermal stability of TPI^{Q181P} using differential scanning fluorimetry. Here, we find that TPI^{Q181P}, TPI^{E105D} and the wild-type control exhibit single-phase non-reversible denaturation as observed for other TPI mutants (Roland et al., 2015). Similar to TPI-Df causing mutants TPI^{R189Q} and TPI^{I170V}, but unlike TPI^{E105D}, we observe a significant increase in thermal stability for TPI^{Q181P} (60.42 +/- 0.03°C) over the wild-type control (54.71 +/- 0.04°C) (Figure 2). Further, we observe that incubation with the substrate dihydroxyacetone phosphate results in a stabilization of wildtype TPI as expected, while that effect was significantly reduced in TPI^{Q181P} (Figure 2). This is consistent with a reduced binding affinity in the Q181P variant. Lastly, we tested the stoichiometry of WT, E105D, and QQ181P TPI variants by analytical size exclusion chromatography. We found that WT and Q181P exhibit very similar retention volumes, while the E105D variant appeared to be in monomer-dimer equilibrium (Figure 3A). Together, these results indicate that the pathogenic defect associated with TPI^{Q181P} is not the result of a loss of protein folding, but is instead a loss of catalytic function.

Structure of TPI Q181P

In an effort to reveal the molecular defect associated with the Q181P mutant, we determined the structure of TPI^{Q181P} using x-ray crystallography at 1.3 Å resolution (see Table 1 and Material and Methods for a complete description of the crystallization and structure determination process). Crystals were obtained in conditions similar to previous TPI structures, belonging to space group $P2_12_12_1$ and contain one TPI dimer in the asymmetric unit. Comparing the structures of wild type (Roland et al., 2015) and TPI^{Q181P}, we find that they are highly similar overall as expected with an all atom r.m.s.d. of 0.24 Å, demonstrating that the overall fold of TPI was not disturbed by the mutation. We did find differences however in three important regions of the TPI structure. The first is within the catalytic lid, which we found to be disordered within the TPI^{Q181P} structure. We observed this in both subunits of the dimer although the affected regions were not identical, with residues 170-177 being disordered in the A subunit, while residues 172-179 were disordered in subunit B. Electron density was clearer for the P181 residue in subunit A (Figure 3C inset), and thus we use this subunit in our figures and description unless noted. Biologically important TPI residues are contained within the disordered region including I170, which enhances catalysis by excluding water within the active site (Richard et al., 2016; Roland et al., 2015) and whose mutation to valine results in TPI Df (Arya, Lalloz, Bellingham, & Layton, 1997). Also affected are residues 173-175 which form the

C-terminal hinge and impact catalytic efficiency (Kursula et al., 2004; Sun & Sampson, 1998). Lastly, A178 was disordered in the B subunit. This residue impacts catalytic efficiency and an A178L mutation has been shown to shift TPI into the closed conformation (Alahuhta, Casteleijn, Neubauer, & Wierenga, 2008). Increased mobility of these key residues found disordered in the TPI^{Q181P} mutant, provides a molecular rationale for the decrease in substrate affinity we observe biochemically (Figure 2C).

We also observe changes at the C-terminal hinge in the TPI^{Q181P} structure. Prominently, P181 introduces a kink in the main chain at the beginning of helix 6. This disrupts hydrogen bonding interactions that occur between Q181 and T178 in the wild-type structure. These interactions are important as they stabilize the beginning of helix 6 but also help orient residues preceding 178 and thereby directly influence the position of the catalytic lid. A proline at position 181 not only disrupts these interactions but introduces a kink in the main chain which prevents residues 177-181 from adopting the helical conformation observed in wild-type TPI structures. Importantly, this disruption is not observed in the structure of the E105D variant (Figure 4A) . Residues 177-181 are observed in a helical conformation in both the open and closed orientation of the catalytic lid, demonstrating that the defect observed is not merely altering the equilibrium between the open and closed states but is instead grossly affecting the C-terminal hinge and catalytic lid (Figure 4A).

Lastly, differences in TPI structure extend into the catalytic site. We crystallized TPI^{Q181P} in the presence of bromide, which we have shown previously will localize in the active site along with a phosphate abstracted from solution. In wild-type TPI, this promotes the closed conformation, with concomitant changes in the key catalytic residues E165 and S96, which are also observed in the E105D variant (Figure 4A-B). In our TPI^{Q181P} structure, however, we observe only partial occupancy for bromide ions, and no phosphates are observed. Further, we find residues E165 and S96 have adopted the open conformation (Figure 4B). All of these results point towards a defect in catalytic lid coordination for TPI^{Q181P}.

Mutant TPI protein levels

The TPI^{Q181P} protein retains less than 10% of the catalytic activity of wild type protein and the molecular defects associated with the Q to P amino acid substitution are consistent with impaired catalysis. However, other mutations in *TPI1* that reduce catalysis are not inherently pathogenic unless protein levels are also reduced (Segal et al., 2019). Thus, we examined protein levels in compound heterozygous TPI^{Q181P}/TPI^{E105D} patient cells. Western blot using

patient fibroblasts demonstrate reduced TPI in patient cells compared to wild type levels (Figure 5). Interestingly, both heterozygous *TPI*^{Q181P}/+ and *TPI*^{E105D}/+ parent cells exhibit a significant but modest reduction in TPI levels (Figure 5). These data are consistent with *TPI*^{Q181P} being a pathogenic mutation that results in both a decrease in protein activity and overall levels, likely through accelerated turnover of the protein.

Resveratrol and Itavastatin increase TPI levels in TPIQ181P/E105D cells

Using a human cellular HEK model of TPI Df expressing fluorescently tagged TPI^{E105D}, the NIH clinical collection drug library was screened to identify compounds that increase mutant TPI levels (Vogt et al., 2021). Using this high-throughput assay resveratrol, a natural supplement, and several statins were identified as potential therapies for TPI Df (Vogt et al., 2021). We asked whether these compounds similarly increase TPI levels in compound heterozygous patient cells. Western blots of *TPI*^{Q181P}/*TPI*^{E105D} patient cells demonstrate that both resveratrol and itavastatin increase TPI levels by ~ 50%, relative to DMSO treated patient cells (Figure 6).

Methods

Human TPI Purification and analytical gel filtration chromatography. Coding sequences for hTPI wild type and mutants were inserted into pLC3 vectors for recombinant expression as a TEV-cleavable His_6-MBP fusion protein and confirmed by sequencing. Expression was performed in codon+ RIPL *E.coli*, using autoinduction media(Studier, 2005) at room temperature for 24 hours. Cells were lysed via homogenization in 25 mM Tris pH 8, 500 mM NaCl, 10% Glycerol, 5 mM imidazole and 1mM β-ME, and cellular debris removed by centrifugation at 30,000 *x g*. TPI protein was then purified by nickel affinity chromatography, followed by cleavage with TEV protease to remove the His-MBP tag. A second round of nickel affinity purification, followed by anion-exchange and gel filtration chromatography were then performed. Peak fractions were concentrated to 6-8 mg/ml prior to crystallization.

Analytical gel filtration chromatography was performed using an analytical S200 at a TPI concentration of 1.5 mg/ml for each TPI variant. Buffering conditions were 20 mM Tris pH 8, 200 mM NaCl, and 1 mM β-ME. Note: The classical convention for numbering TPI amino acids does not include the start methionine, thus, E105D is AKA E104D in some previous published papers. We have used actual numbering throughout this manuscript as the classical convention

complicates structural discussions with a protein that has a start methionine and also because amino acids 181 and 182 in the human TPI1 wild type protein are both glutamine (Q).

Crystallization and structure determination. Crystals of hTPI^{Q181P} were grown using the sitting drop vapor diffusion method at 4°C. The crystals grew overnight in a drop consisting of 1µL of protein (at a concentration of 6-8 mg/ml) and 2µL of a well solution containing 14-15% PEG 2000 MME and 50 mM potassium bromide as in previous structural studies (Roland et al., 2015; Roland et al., 2019; Roland et al., 2013). The crystals were then cryoprotected in 36% PEG 2000 MME and flash frozen in liquid nitrogen prior to X-ray diffraction. Diffraction data were collected at beamline 31-IDD at Argonne National Labs and processed and scaled via AutoPROC (Vonrhein et al., 2011) using $I/\sigma I$ >2.0 and CC(1/2) >0.3 as cutoffs. Crystals belong to space group $P2_12_12_1$ with a=73.2, b=77.8, and c=84.3 Å. Phases were estimated using molecular replacement within Phenix (Adams et al., 2010) using wtTPI as a search model (4POC) (Roland et al., 2015) and used to calculate an initial map. The initial model was then improved through rounds of model building in COOT (Emsley, Lohkamp, Scott, & Cowtan, 2010) and positional and anisotropic B-factor refinement within Phenix. Model quality was assessed using MolProbity within Phenix. Structure factors and atomic coordinates have been deposited into the PDB (www.rcsb.org) under 7RDE

Differential Scanning Fluorometry. The thermal stability of hTPI WT and Q181P mutant was determined using differential scanning fluorimetry. TPI Q181P and TPI WT protein was diluted to 0.1 and 0.25 mg/mL respectively in a buffer containing 20mM HEPES pH 7.5 15mM NaCl, 5% glycerol, 1mM 2-mercaptoethanol and 1X Glo-Melt fluorescent dye, using ROX as a passive reference. Four replicates were performed using the Thermo-Fisher QuantStudio-3 Real-Time PCR and a temperature gradient of 30-95 °C. Fluorescence of Glo-Melt was measured at 520nm, and the melting temperature (T_M) defined as the peak of the derivative curve. To assess the effect of the Q181P mutant on the ability to interact with substrate, 10mM DHAP was added into the reaction, and the resulting Tm compared to the same protein in which the same volume of vehicle (water) had been added.

Protein activity assays. Purified TPI (1ng) was examined for isomerase activity using an NADH-linked assay previously described (Roland et al., 2013; Williams et al., 1999). Reactions were run in triplicate over a range of 0.095 to 4.23mM GAP (Sigma Aldrich, St. Louis, MO, USA)

with an accompanying no GAP control. Absorbance data were collected using a Spectra Max Plus 384 microplate reader (Molecular Devices, Sunnyvale, CA, USA). Enzyme kinetics were evaluated in the initial linear phase of each reaction and were fit to the Michaelis-Menten equation using nonlinear regression in GraphPad V8 Prism (GraphPad Software, La Jolla, CA, USA).

Culturing Patient Fibroblasts. Patient and parental fibroblasts were obtained via skin punch (Duke University Health System IRB protocol number 00014158). The cells were de-identified, genotype confirmed and tested for mycoplasma using Invitrogen mycofluor mycoplasma detection kit (Fisher cat. no. M7006). Fibroblasts are frequently retested for mycoplasma and were cultured using standard methods (37C, 5% CO_2) in complete media (DMEM with 10% serum, 100 U penicillin/100 µg streptomycin/ml (Lonza), 2 mM L-glutamine (Gibco) and supplemental non-essential amino acids (Gibco).

Western Blotting. Patient and control fibroblast Western blotting was performed as previously reported (Vogt et al., 2021). Briefly, cells were trypsinized (0.05% for 5 min), pelleted, resuspended in RIPA buffer with protease inhibitors (PMSF (100 µM), Leupeptin (1 µg/µL), Pepstatin A (0.5 µg/µL) and pulse sonicated. BCA assays (Pierce) quantified protein concentrations and immunoblotting of whole protein cell lysates resolved by SDS-PAGE (12%), transferred onto 0.45 µm PVDF membrane using anti-TPI (1:5000; rabbit polyclonal FL-249; Santa Cruz Biotechnology sc-30145) or anti-beta-tubulin (1:1000; mouse polyclonal E7-C; Developmental Studies Hybridoma Bank) diluted in Odyssey Blocking Buffer (Licor). Scanned images were quantified digitally (Image Studio Ver 5.2 software), TPI levels were normalized to the loading control, and differences in TPI expression were evaluated by a two-tailed Student's *t*-test.

Discussion

TPI^{Q181P} is a novel TPI1 mutation that results in TPI Df, at least in the *TPI*^{Q181P}/*TPI*^{E105D} combination observed in these patients. The *TPI*^{Q181P} protein exhibits a marked reduction in biochemical activity and a significant reduction in TPI protein was observed in *TPI*^{Q181P}/*TPI*^{E105D} cells. Certainly, the data are consistent with TPI^{Q181P} being a pathogenic *TPI1* allele capable of causing or contributing to TPI Df. Although the patients are severely affected and the symptoms

rapidly progressed, their disease course is less severe than other compound heterozygotes or *TPI*^{E105D} homozygotes. Notable is the severity of the muscular symptoms yet the lack of childhood-onset cognitive impairment. This suggests genetic complementation may be occurring between these alleles leading to a reduction in symptoms within parts of the nervous system similar to what was observed in TPI $^{\text{delta Cat/sgk}}$ animals (Roland et al., 2013).

The severe deficits observed in patients containing TPI^{Q181P} are mirrored at the molecular level. The high-resolution crystal structure of TPI^{Q181P} shows that this substitution affects both critical active site residues and positioning of the catalytic lid, effectively uncoupling their coordinated movements. This is borne out biochemically as well. Further, the increase in K_m suggests a loss of substrate-protein interactions, the precise nature of which cannot be observed crystallographically. Ultimately, we show here that discoordination of the catalytic lid caused by the TPI^{Q181P} mutant, is correlated with increased rates of protein turnover in cells. It is possible that enhanced accessibility of residues in the catalytic lid is causing TPI^{Q181P} to be recognized by protein quality control machinery, thereby increasing rates of protein turnover.

TPI Df is a severe, rapidly progressive, untreatable disease and there is a pressing need to develop therapies. One approach is to inhibit the proteins that underlie the accelerated turnover of mutant TPI. Genetic screening has found dozens of proteins putatively involved in mutant TPI turnover, suggesting there are numerous possible pharmacologic targets (Hrizo et al., 2021). The premise of this approach is that it is likely easier block degradation of the protein being made by the cell than to correct the dysfunction that results from a severe alteration in intermediate metabolism. TPI is an essential enzyme in organisms from *E. coli* to humans and the TPI Df pathogenic mutations studied so far encode proteins with greatly reduced activity, but more significantly, have impaired proteolytic cleavage, dimer stability, and thermal stability. These findings suggest that increasing the amount of mutant protein may be of therapeutic value, which is supported by results in animal models of TPI Df. Increasing mutant protein, even modestly, using genetic or pharmacologic approaches improves longevity and locomotor function (Hrizo & Palladino, 2010; Seigle et al., 2008). Importantly, resveratrol and itavastain were previously shown to increase mutant TPI protein in TPI^{E105D} homozygous patient cells and here we show that they similarly increase mutant protein levels in *TPI*^{Q181P}/*TPI*^{E105D} patient cells. Given the presence of mitochondrial complex I deficiency in the affected siblings described herein and previously described mitochondrial dysfunction in TPI Df flies (Hrizo et al., 2013),

resveratrol could be beneficial in TPI Df through its antioxidant effects (de la Lastra & Villegas, 2007) Although these data suggest resveratrol and itavastatin could be of therapeutic value, there remains a pressing need for a mammalian model to test the efficacy *in vivo*. Additionally, although it is likely that increasing the amount of mutant protein will offer immediate benefits in terms of symptomatic relief, the long-term effect of such an approach is not known.

TPI^{E105D} is the "common" mutation, and it is the only known human *TPI1* mutation that results in disease as a homozygote. Numerous patients have been reported that are compound heterozygotes, typically with one of the alleles being *TPI*^{E105D}. One such compound heterozygous patient with a *TPI*^{R190Q}/*TPI*^{E105D} allelic combination, has the most severe presentation that has been reported (Roland et al., 2019). *TPI*^{Q181P}/*TPI*^{E105D} is the latest compound heterozygous combination reported, and while the disease still presents with significant symptoms, it does appear to have a milder form than the classic, and does not appear to have significant childhood-onset cognitive impairment. It is possible that these alleles genetically complement, particularly in the nervous system, resulting in the less-severe symptoms, however, the basis of this apparent tissue-specificity is not understood. Although this is a reasonable hypothesis and is similar to what was observed in *TPI*$^{deltaCat/sgk}$ alleles in *Drosophila*, additional studies are needed. Although the patient fibroblast studies here are important, studies with nervous tissues are needed to better elucidate the basis of the apparent genetic complementation.

Pathogenesis in compound heterozygous patients is difficult to study. This is particularly true with a protein that forms a dimer. Theoretically within *TPI*^{Q181P}/*TPI*^{E105D} patient cells *TPI*^{Q181P} and *TPI*^{E105D} homodimers, as well as *TPI*^{Q181P}-*TPI*^{E105D} heterodimers are formed. In fact, there is evidence of heterodimers in a TPI compound heterozygote animal model (Roland et al., 2013). We have measured biochemical activity of the homodimer protein and determined protein levels in the compound heterozygous patient cells, but a much better understanding of pathogenesis could be achieved with biochemical activity and a structure of the *TPI*^{Q181P}-*TPI*^{E105D} heterodimer and with a *TPI*^{Q181P}-*TPI*^{E105D} animal model that would enable direct studies of pathogenesis within neuromuscular tissues.

Acknowledgements

This research used resources of the Advanced Photon Source, a U.S. Department of Energy (DOE) Office of Science User Facility operated for the DOE Office of Science by Argonne National Laboratory under Contract No. DE-AC02-06CH11357. Use of the Lilly Research Laboratories Collaborative Access Team (LRL-CAT) beamline at Sector 31 of the Advanced Photon Source was provided by Eli Lilly Company, which operates the facility. We are grateful to the National Institutes of Health for funding this research project (R21 AG059385, R01 GM103369, R01 HD105311, R01 HD105311, R01 HD104346 and T32 GM133332). We acknowledge the brave patients and generous parents who donated cells for biomedical research.

Declaration of Conflicting Interests

The authors declare the following potential conflicts of interest with respect to the research, authorship, and/or publication of this article: The University of Pittsburgh has filed a provisional patent application on which Drs. Michael Palladino and Stacy Hrizo are listed as inventors. No personal financial benefit has been realized, and there are no pending plans to commercialize that would create a competing financial interest.

References

Works Cited

Adams, P. D., Afonine, P. V., Bunkoczi, G., Chen, V. B., Davis, I. W., Echols, N., . . . Zwart, P. H. (2010). PHENIX: a comprehensive Python-based system for macromolecular structure solution. *Acta Crystallogr D Biol Crystallogr*, *66*(Pt 2), 213-221. doi:10.1107/S0907444909052925

Alahuhta, M., Casteleijn, M. G., Neubauer, P., & Wierenga, R. K. (2008). Structural studies show that the A178L mutation in the C-terminal hinge of the catalytic loop-6 of triosephosphate isomerase (TIM) induces a closed-like conformation in dimeric and monomeric TIM. *Acta Crystallogr D Biol Crystallogr*, *64*(Pt 2), 178-188. doi:10.1107/S0907444907059021

Arya, R., Lalloz, M. R., Bellingham, A. J., & Layton, D. M. (1997). Evidence for founder effect of the Glu104Asp substitution and identification of new mutations in triosephosphate isomerase deficiency. *Hum Mutat*, *10*(4), 290-294. doi:10.1002/(SICI)1098-1004(1997)10:4<290::AID-HUMU4>3.0.CO;2-L

Banner, D. W., Bloomer, A. C., Petsko, G. A., Phillips, D. C., & Pogson, C. I. (1972). Crystallographic studies of chicken triose phosphate isomerase. *Cold Spring Harb Symp Quant Biol*, *36*, 151-155. doi:10.1101/sqb.1972.036.01.021

Cabrera, N., Torres-Larios, A., Garcia-Torres, I., Enriquez-Flores, S., & Perez-Montfort, R. (2018). Differential effects on enzyme stability and kinetic parameters of mutants related to human triosephosphate isomerase deficiency. *Biochim Biophys Acta Gen Subj, 1862*(6), 1401-1409. doi:10.1016/j.bbagen.2018.03.019

Celotto, A. M., Frank, A. C., Seigle, J. L., & Palladino, M. J. (2006). Drosophila model of human inherited triosephosphate isomerase deficiency glycolytic enzymopathy. *Genetics, 174*(3), 1237-1246. doi:10.1534/genetics.106.063206

Conway, A. J., Brown, F. C., Hortle, E. J., Burgio, G., Foote, S. J., Morton, C. J., . . . Curtis, D. J. (2018). Bone marrow transplantation corrects haemolytic anaemia in a novel ENU mutagenesis mouse model of TPI deficiency. *Dis Model Mech, 11*(5). doi:10.1242/dmm.034678

de la Lastra, C. A., & Villegas, I. (2007). Resveratrol as an antioxidant and pro-oxidant agent: mechanisms and clinical implications. *Biochem Soc Trans, 35*(Pt 5), 1156-1160. doi:10.1042/BST0351156

De La Mora-De La Mora, I., Torres-Larios, A., Mendoza-Hernandez, G., Enriquez-Flores, S., Castillo-Villanueva, A., Mendez, S. T., . . . Reyes-Vivas, H. (2013). The E104D mutation increases the susceptibility of human triosephosphate isomerase to proteolysis. Asymmetric cleavage of the two monomers of the homodimeric enzyme. *Biochim Biophys Acta, 1834*(12), 2702-2711. doi:10.1016/j.bbapap.2013.08.012

Emsley, P., Lohkamp, B., Scott, W. G., & Cowtan, K. (2010). Features and development of Coot. *Acta Crystallogr D Biol Crystallogr, 66*(Pt 4), 486-501. doi:10.1107/S0907444910007493

Hrizo, S. L., Eicher, S. L., Myers, T. D., McGrath, I., Wodrich, A. P. K., Venkatesh, H., . . . Palladino, M. J. (2021). Identification of protein quality control regulators using a Drosophila model of TPI deficiency. *Neurobiol Dis, 152*, 105299. doi:10.1016/j.nbd.2021.105299

Hrizo, S. L., Fisher, I. J., Long, D. R., Hutton, J. A., Liu, Z., & Palladino, M. J. (2013). Early mitochondrial dysfunction leads to altered redox chemistry underlying pathogenesis of TPI deficiency. *Neurobiol Dis, 54*, 289-296. doi:10.1016/j.nbd.2012.12.020

Hrizo, S. L., & Palladino, M. J. (2010). Hsp70- and Hsp90-mediated proteasomal degradation underlies TPI sugarkill pathogenesis in Drosophila. *Neurobiol Dis, 40*(3), 676-683. doi:10.1016/j.nbd.2010.08.011

Kursula, I., Salin, M., Sun, J., Norledge, B. V., Haapalainen, A. M., Sampson, N. S., & Wierenga, R. K. (2004). Understanding protein lids: structural analysis of active hinge mutants in triosephosphate isomerase. *Protein Eng Des Sel, 17*(4), 375-382. doi:10.1093/protein/gzh048

Lolis, E., Alber, T., Davenport, R. C., Rose, D., Hartman, F. C., & Petsko, G. A. (1990). Structure of yeast triosephosphate isomerase at 1.9-A resolution. *Biochemistry, 29*(28), 6609-6618. doi:10.1021/bi00480a009

Massi, F., Wang, C., & Palmer, A. G., 3rd. (2006). Solution NMR and computer simulation studies of active site loop motion in triosephosphate isomerase. *Biochemistry, 45*(36), 10787-10794. doi:10.1021/bi060764c

Pretsch, W. (2009). Triosephosphate isomerase activity-deficient mice show haemolytic anaemia in homozygous condition. *Genet Res (Camb), 91*(1), 1-4. doi:10.1017/S0016672308009944

Richard, J. P., Amyes, T. L., Malabanan, M. M., Zhai, X., Kim, K. J., Reinhardt, C. J., . . . Gulick, A. M. (2016). Structure-Function Studies of Hydrophobic Residues That Clamp a Basic Glutamate Side Chain during Catalysis by Triosephosphate Isomerase. *Biochemistry, 55*(21), 3036-3047. doi:10.1021/acs.biochem.6b00311

Rodriguez-Almazan, C., Arreola, R., Rodriguez-Larrea, D., Aguirre-Lopez, B., de Gomez-Puyou, M. T., Perez-Montfort, R., . . . Torres-Larios, A. (2008). Structural basis of human triosephosphate isomerase deficiency: mutation E104D is related to alterations of a conserved water network at the dimer interface. *J Biol Chem, 283*(34), 23254-23263. doi:10.1074/jbc.M802145200

Roland, B. P., Amrich, C. G., Kammerer, C. J., Stuchul, K. A., Larsen, S. B., Rode, S., . . . Palladino, M. J. (2015). Triosephosphate isomerase I170V alters catalytic site, enhances stability and induces pathology in a Drosophila model of TPI deficiency. *Biochim Biophys Acta, 1852*(1), 61-69. doi:10.1016/j.bbadis.2014.10.010

Roland, B. P., Richards, K. R., Hrizo, S. L., Eicher, S., Barile, Z. J., Chang, T. C., . . . Palladino, M. J. (2019). Missense variant in TPI1 (Arg189Gln) causes neurologic deficits through structural changes in the triosephosphate isomerase catalytic site and reduced enzyme levels in vivo. *Biochim Biophys Acta Mol Basis Dis, 1865*(9), 2257-2266. doi:10.1016/j.bbadis.2019.05.002

Roland, B. P., Stuchul, K. A., Larsen, S. B., Amrich, C. G., Vandemark, A. P., Celotto, A. M., & Palladino, M. J. (2013). Evidence of a triosephosphate isomerase non-catalytic function crucial to behavior and longevity. *J Cell Sci, 126*(Pt 14), 3151-3158. doi:10.1242/jcs.124586

Roland, B. P., Zeccola, A. M., Larsen, S. B., Amrich, C. G., Talsma, A. D., Stuchul, K. A., . . . Palladino, M. J. (2016). Structural and Genetic Studies Demonstrate Neurologic Dysfunction in Triosephosphate Isomerase Deficiency Is Associated with Impaired Synaptic Vesicle Dynamics. *PLoS Genet, 12*(3), e1005941. doi:10.1371/journal.pgen.1005941

Segal, J., Mulleder, M., Kruger, A., Adler, T., Scholze-Wittler, M., Becker, L., . . . Ralser, M. (2019). Low catalytic activity is insufficient to induce disease pathology in triosephosphate isomerase deficiency. *J Inherit Metab Dis, 42*(5), 839-849. doi:10.1002/jimd.12105

Seigle, J. L., Celotto, A. M., & Palladino, M. J. (2008). Degradation of functional triose phosphate isomerase protein underlies sugarkill pathology. *Genetics, 179*(2), 855-862. doi:10.1534/genetics.108.087551

Studier, F. W. (2005). Protein production by auto-induction in high density shaking cultures. *Protein Expr Purif, 41*(1), 207-234. doi:10.1016/j.pep.2005.01.016

Sun, J., & Sampson, N. S. (1998). Determination of the amino acid requirements for a protein hinge in triosephosphate isomerase. *Protein Sci, 7*(7), 1495-1505. doi:10.1002/pro.5560070702

Vogt, A., Eicher, S. L., Myers, T. D., Hrizo, S. L., Vollmer, L. L., Meyer, E. M., & Palladino, M. J. (2021). A High-Content Screening Assay for Small Molecules That Stabilize Mutant Triose Phosphate Isomerase (TPI) as Treatments for TPI Deficiency. *SLAS Discovery*. doi:Artn 10.1177/24725552211018198

Vonrhein, C., Flensburg, C., Keller, P., Sharff, A., Smart, O., Paciorek, W., . . . Bricogne, G. (2011). Data processing and analysis with the autoPROC toolbox. *Acta Crystallogr D Biol Crystallogr, 67*(Pt 4), 293-302. doi:10.1107/S0907444911007773

Wierenga, R. K., Noble, M. E., & Davenport, R. C. (1992). Comparison of the refined crystal structures of liganded and unliganded chicken, yeast and trypanosomal triosephosphate isomerase. *J Mol Biol, 224*(4), 1115-1126. doi:10.1016/0022-2836(92)90473-w

Williams, J. C., Zeelen, J. P., Neubauer, G., Vriend, G., Backmann, J., Michels, P. A., . . . Wierenga, R. K. (1999). Structural and mutagenesis studies of leishmania triosephosphate isomerase: a point mutation can convert a mesophilic enzyme into a superstable enzyme without losing catalytic power. *Protein Eng, 12*(3), 243-250. doi:10.1093/protein/12.3.243

Zhang, Z., Sugio, S., Komives, E. A., Liu, K. D., Knowles, J. R., Petsko, G. A., & Ringe, D. (1994). Crystal structure of recombinant chicken triosephosphate isomerase-phosphoglycolohydroxamate complex at 1.8-A resolution. *Biochemistry, 33*(10), 2830-2837. doi:10.1021/bi00176a012

Figures

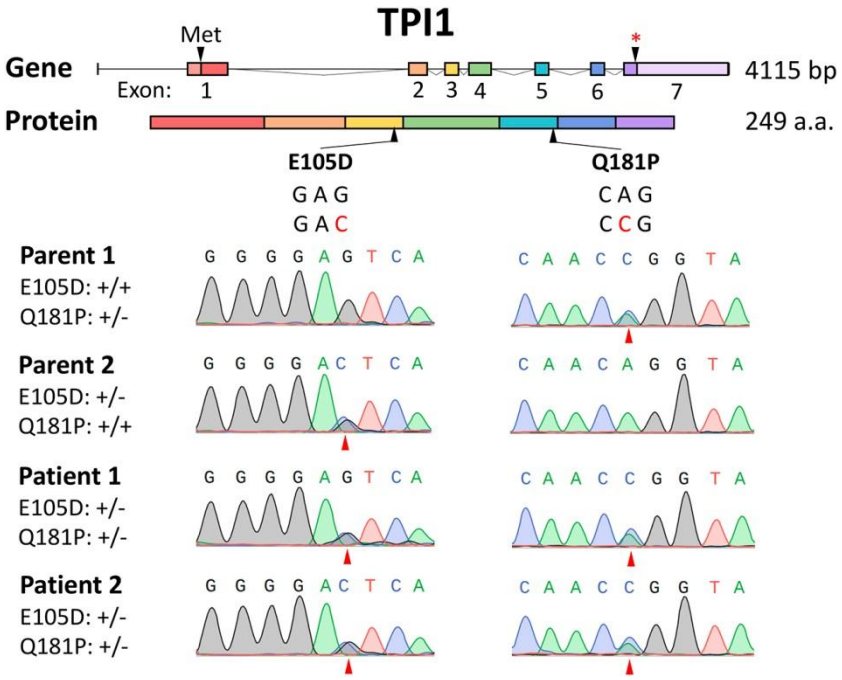

Figure 1: Sequence analysis of *TPI1* locus. A) Cartoon of the TPI gene showing the location of each mutation. B) Chromatographic data demonstrating the mutations observed and confirming both patients are compound heterozygotes for the Q181P and E105D mutations.

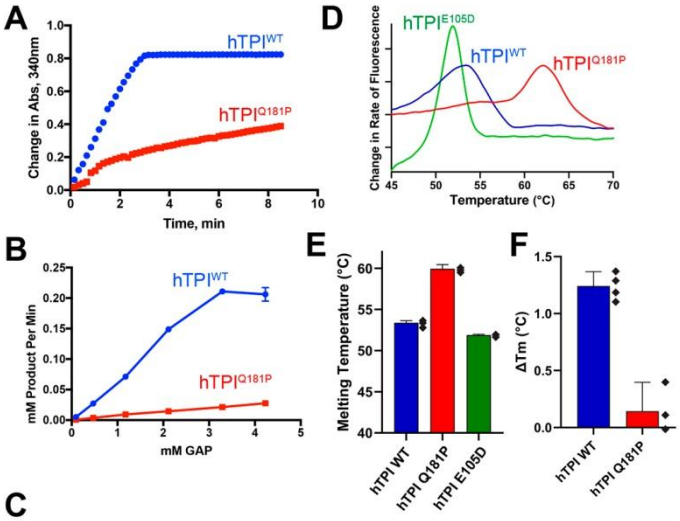

C

	hTPI^{WT}	hTPI^{Q181P}
Km (GAP,mM)	6.791	21.380
Vmax (GAP, mM prod./min)	0.583	0.165
Kcat (GAP s^{-1})	2020.38	572.05
Kcat/Km (GAP, $M^{-1}s^{-1}$)	297,500	26,760 (<9% of WT)

Figure 2: TPI^{Q181P} exhibits reduced substrate binding and rate of catalysis compared to the wildtype enzyme. A) TPI activity from a spectrophotometric enzyme linked assay of 1ng purified TPI enzyme in the reaction with 2.115 mM of GAP. B) The absorbance data was used to determine the mM of product formed per minute by 1ng of TPI enzyme at varying concentrations of the substrate GAP. The average for each concentration of GAP is shown, N= 3. C) Prism calculated V_{Max}, K_M and K_{CAT}. D) Representative curves from differential scanning fluorimetry (DSF) showing increased thermal stability for TPI^{Q181P} (red) as compared to WT (blue) and TPI^{E105D} (green). E) Quantification of DSF from both WT, Q181P, and E105D TPI variants (n=4). Error bars are standard error of the mean, and the p-value was <0.00001. F) Change in Tm from DSF measurements of WT and Q181P with the addition of 10mM DHAP. Error bars represent standard error of the mean (n=4), Two sample T-test was used to determine significance, *** indicates p-value<0.00001.

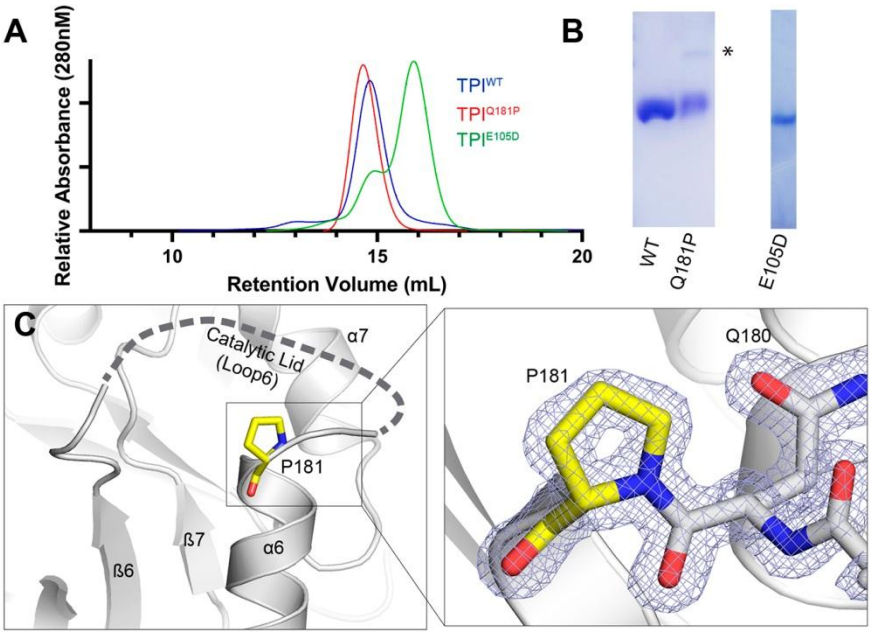

Figure 3: Biophysical and structural characterization of TPI^{Q181P}. A) Size exclusion chromatography demonstrating that both wt and TPI^{Q181P} proteins are dimeric and show no gross changes in overall structure or stoichiometry. TPI^{E105D} appears to exist in a monomer-dimer equilibrium under these conditions. B) Purified TPI variants used in this study. C) The catalytic lid region from the structure of TPI^{Q181P}. Electron density for P181 is shown (inset), however the catalytic lid is largely disordered.

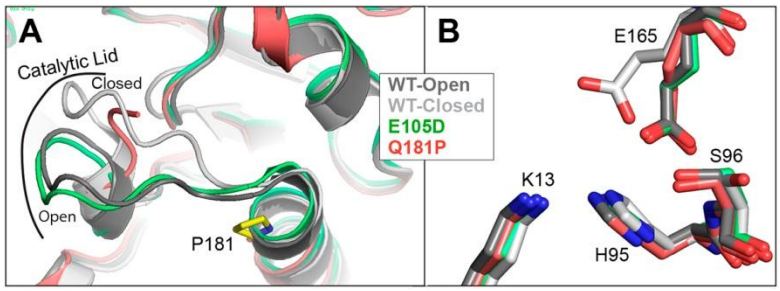

Figure 4: TPI^{Q181P} results in discoordination of the catalytic lid. A) Superposition of TPI^{Q181P} (red) with TPI^{WT} structures in the open (dark grey) and closed state (light grey), as well as TPI^{E105D} (green). P181 is highlighted in yellow for reference. B) The positions of catalytic residues K13, H95, S96, and E165 from the same superposition are shown and colored as in (A). The positions of residues E165 and S96 indicate that these residues are adopting the open conformation in TPI^{Q181P}

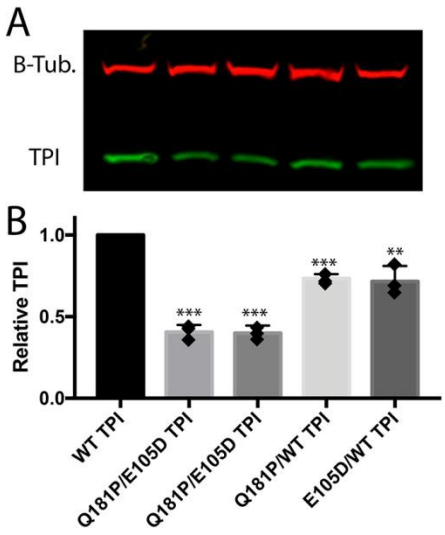

Figure 5: Western Blot data from patient fibroblasts compared with heterozygous unaffected parental controls. A) Representative Western blot of lysates quantified in B). Both patients exhibited ~ 40% of normal TPI levels. N=3, Two-tailed student's *t*-test was used to determine significance. *** is P<0.001, ** is P<0.005 from WT. Note: this is significantly higher than the ~ 10% that was observed in R190Q/E105D patient with a much more severe disease course (Roland et al., 2019).

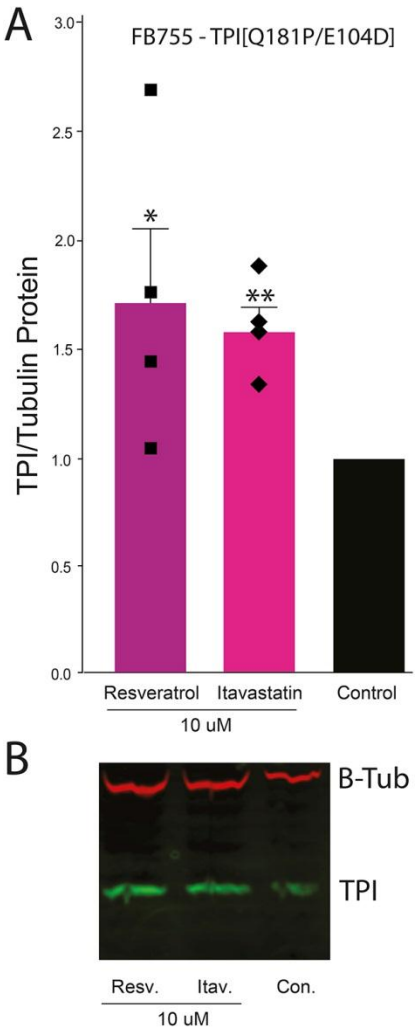

Figure 6: Resveratrol and Itavastatin improve TPI levels by Western Blot in *TPI*$^{Q181P/E105D}$ patient fibroblasts. Significant increases in TPI protein was observed in patient cells relative to control. Shown is mean ± SEM of four biological replicates. n=4. Two-tailed Student's *t*-test was used to determine significance (* $p<0.05$; ** $p<0.005$).

Table 1. Data collection and refinement statistics

	TPI-Q181P
Data collection	
Space group	$P2_12_12_1$
Cell dimensions	
a, *b*, *c* (Å)	73.2, 77.8, 84.3
Resolution (Å)	57.2-1.308 (1.331-1.308)
Unique reflections	115,131 (5,679)
R_{merge}	0.079 (0.853)
R_{pim}	0.033 (0.510)
$I/\sigma I$	13.3 (2.1)
Completeness (%)	98.8 (98.5)
Redundancy	6.6 (6.3)
CC(1/2)	0.998 (0.701)
Refinement	
Resolution (Å)	57.2-1.308 (1.331-1.308)
R_{work} / $R_{free\ (\%)}$	13.7/16.2 (22.7/24.4)/
Non-hydrogen atoms	
Protein	3614
Water	553
Ions	3
B-factors	16.75
Protein	15.07
Ion	17.41
Water	27.60
R.m.s. deviations	
Bond lengths (Å)	0.009
Bond angles (°)	1.032
Ramachandran	
Favored	97.45
Allowed	2.55
Outliers	0.00
Clashscore	0.55

[a]Values in parentheses are for highest-resolution shell.

[b]$R_{pim} = \Sigma_h [1/(n_h-1)]^{1/2} * \Sigma_i |<I_h> - I_{h,i}| / \Sigma_h \Sigma_i I_{h,i}$ where *h* represents unique reflections, *i* are their symmetry-equivalents, n_h denotes the multiplicity, <I> is the average intensity of multiple measurements.

[c]$R_{work} = \Sigma_{hkl}||F_{obs}(hkl)|| - F_{calc}\ (hkl)||/\Sigma_{hkl}|F_{obs}(hkl)|$.

[d]R_{free} represents the cross-validation R factor for reflections against which the model was not refined. A total of 1,982 reflections are contained in this test set.

A)

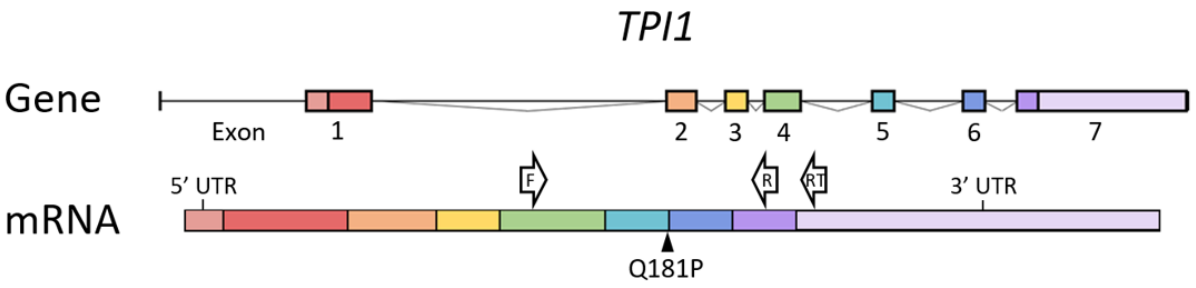

B)

	Splice Recognition Sequence		ASSP Score
	Exon 5	Intron	
Normal	CAG	GTAA	13.884
Q181P	CCG	GTAA	9.964

C)

Splicing Variant	Expected Length of PCR Product (bp)
Normal	351
Exon 5 Skipped	263

D)

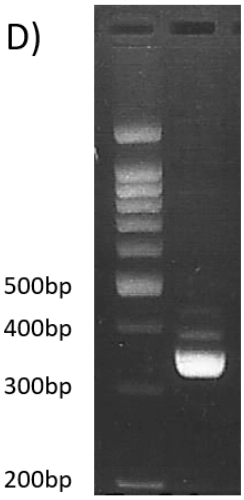

Fig. S1. *TPI1*^{Q181P} mutation alters the exon 5 splice donor sequence. **A)** Structure of *TPI1* gene and mRNA. Location of reverse transcription (RT) and PCR primers are noted. **B)** The splice recognition sequence is altered by *TPI*^{Q181P} per Alternative Splice Site Predictor (ASSP), where higher scores indicate a better splice site (Wang, M., & Marin, A. (2006) Characterization and prediction of alternative splice sites. Gene, 366(2), 219-227. doi:10.1016/j.gene.2005.07.015). **C)** *TPI*^{Q181P} was predicted to lead to skipping of exon 5 using varSEAK (JSI Medical Systems). The potential lengths of PCR products with or without exon 5 skipping are noted in the chart. **D)** RT-PCR was used to investigate splice variation of *TPI1*^{Q181P}. Whole RNA was isolated from *TPI*$^{WT/Q181P}$ human fibroblasts (Qiagen RNeasy Mini Kit catalog no. 74104). cDNA was generated (Invitrogen SuperScript III First-Strand Synthesis catalog no. 18080051) using a gene-specific reverse transcription primer. Exons 4-7 of *TPI1*^{Q181P} was PCR amplified (Invitrogen Platinum Taq DNA Polymerase High Fidelity catalog no. 11304011). PCR amplicons were visualized on a 3% agarose gel with ethidium bromide adjacent to a 100 bp ladder. The major product corresponds to a 351-base pair (bp) product, while there is an absence of a 263 bp product. These data suggest that exon 5 skipping is not prevalent.